Double perovskites overtaking the single perovskites: A set of new solar harvesting materials with much higher stability and efficiency

Jiban Kangsabanik,[1] Vipinraj Sugathan,[2] Anuradha Yadav,[1] Aswani Yella,[2] and Aftab Alam[1,*]
[1]*Department of Physics, Indian Institute of Technology Bombay, Mumbai 400076, India*
[2]*Department of Metallurgical Engineering & Materials Science, Indian Institute of Technology Bombay, Mumbai 400076, India*

(Received 2 February 2018; published 11 May 2018)

Solar energy plays an important role in substituting the ever declining source of fossil fuel energy. Finding novel materials for solar cell applications is an integral part of photovoltaic research. Hybrid lead halide perovskites are one of, if not the most, well sought material in the photovoltaic research community. Its unique intrinsic properties, flexible synthesis techniques, and device fabrication architecture made the community highly buoyant over the past few years. Yet, there are two fundamental issues that still remain a concern, i.e., the stability in external environment and the toxicity due to Pb. This led to a search for alternative materials. More recently, double perovskite [$A_2BB'X_6$ (X=Cl, Br, I)] materials have emerged as a promising choice. Few experimental synthesis and high throughput computational studies have been carried out to check for promising candidates of this class. The main outcome from these studies, however, can essentially be summarized into two categories: (i) either they have an indirect band gap or (ii) a direct but large optical band gap, which is not suitable for solar devices. Here we propose a large set of stable double perovskite materials, $Cs_2BB'X_6$ (X=Cl, Br, I), which show indirect to direct band gap transition via small Pb^{+2} doping at both B and B' sites. This is done by careful band (orbital) engineering using first-principles calculations. This kind of doping has helped to change the topology of the band structure, triggering an indirect to direct transition that is optically allowed. It also reduces the band gap significantly, bringing it well into the visible region. We also simulated the optical absorption spectra of these systems and found a comparable/higher absorption coefficient and solar efficiency with respect to the state of the art photovoltaic absorber material $CH_3NH_3PbI_3$. A number of materials $Cs_2(B_{0.75}Pb_{0.25})(B'_{0.75}Pb_{0.25})X_6$ (for various combinations of B, B', and X) are found to be promising, some with better stability and solar efficiency than $CH_3NH_3PbI_3$, but with much less toxicity. Experimental characterization of one of the materials, $Cs_2(Ag_{0.75}Pb_{0.25})(Bi_{0.75}Pb_{0.25})Br_6$, is carried out. The measured properties such as band gap and chemical stability agree fairly well with the theoretical predictions. This material is shown to be even more stable than $CH_3NH_3PbI_3$, both under sufficient humidity ($\sim$ 55%) and temperature (T = 338 K), and hence has the potential to become a better candidate than the state of the art materials.

DOI: 10.1103/PhysRevMaterials.2.055401

I. INTRODUCTION

As most of the fossil fuel energy sources are declining towards an end, the quest for natural, renewable energy sources is becoming an area of utmost importance. At this moment, solar energy plays an integral role, therefore the study of photovoltaics is one of the most important fields of research. Finding novel materials for solar cell applications is a fundamental part of this field. Hybrid lead halide perovskites are among the most well sought materials in the photovoltaic research community in recent past. Starting from 3.8% efficiency at the beginning in 2009 [1], they have now reached a reported efficiency of 22.1% within only 7 years [2]. Their unique intrinsic properties as well as very flexible synthesis technique and device fabrication architecture made the community highly buoyant over the past few years. Yet, there remain two fundamental issues, i.e., the stability in external environment and the toxicity due to Pb. Various studies, both at experimental and computational level, have been carried out to solve these. From the device fabrication perspective, improving the quality of the film using different conducting layers, encapsulation, etc., helped to increase the stability to some extent. Also, changing the organic cation and mixing different halides helped to slightly improve the stability, but compromised the efficiency and other properties in many cases [3]. Next, to remove the toxicity, many people have tried to find a suitable substitution of Pb at the B site of the ABX_3 structure [4]. But that either resulted in a higher band gap value (in case of alkaline earth metals) [5], which is unsuitable as an absorber material, or they turned out to be even more unstable (for Sn and Ge substitutions) [6,7]. This led to a search for alternative materials to achieve both necessary criteria. In 2016, Volonakis *et al.* suggested heterovalent substitution of Pb with one +3 and one +1 element resulting in a double perovskite structure [8]. Slavney *et al.* first synthesized and reported $Cs_2AgBiBr_6$ to have long carrier lifetime and band gap in the visible range [9]. But the material shows an indirect nature of band gap with poor absorption properties. In addition, it is prone to high nonradiative recombination loss, making it less suitable for solar harvesting. Next, Volonakis *et al.* reported $Cs_2InAgCl_6$, which although has a direct band gap [10], the gap value is

*aftab@iitb.ac.in

TABLE I. Possible permutations of G-XI elements (Cu, Ag, Au) at B site, and G-XV (Sb, Bi) and G-III (Sc, Y) elements at B' site in forming the double perovskite compound $Cs_2BB'X_6$ (✗= Cl, Br, I). ✓ means the compound satisfies both Goldschmidt's and octahedral tolerance criteria, whereas ✗ represents a structure not satisfying either or both of these criteria.

B \ B′	Sb			Bi			Sc			Y		
	Cl	Br	I	Cl	Br	I	Cl	Br	I	Cl	Br	I
Cu	✓	✗	✗	✓	✗	✗	✓	✗	✗	✓	✗	✗
Ag	✓	✗	✗	✓	✓	✓	✓	✗	✗	✓	✓	✓
Au	✓	✗	✗	✓	✓	✓	✓	✗	✗	✓	✓	✓

on the high violet region. Since then, various computational studies were carried out exploring numerous combinations of halide double perovskites [11–13]. The main outcome from these studies is essentially similar to the two specific cases described above, i.e., either the materials have an indirect band gap or a direct one but with a large optical band gap. Recently, Meng *et al.* in their computational study reported that for most of the direct band gap halide double perovskites, the transition from valence band maximum (VBM) to conduction band minimum (CBM) is optically forbidden. This happens due to the inversion symmetry present in this structure, resulting in VBM and CBM having the same parity [14]. They only found $Cs_2(In,Tl)^{+1}(Sb,Bi)^{+3}X_6$ to be the only class with optically allowed direct band gaps. These compounds are also reported by Zhao *et al.* in their study to have superior theoretical efficiency [13]. But Indium is prone to remain in In^{+3} oxidation state and hence the above compound is literally impossible to form [15]. From the above discussion, one can conclude that, for the double perovskites the next possible avenue should be to find a way to either decrease the optically allowed band gaps or to band engineer an indirect band gap system to achieve a direct band gap. Recently, some studies have been reported to control the nature of the band gap [16,17].

Here, we tried to solve this issue with a different approach. In the perovskite structure ABX_3, the inherent inversion symmetry allows for parity forbidden transitions, which can substantially affect the performance of a solar absorber material. This is precisely the case for most of the double perovskites. In the perovskite structure, the BX_6 octahedra play an important role in dictating various symmetry properties. Tilting or twisting the octahedra can affect the symmetry properties in a particular material. Here, the relative size of A and B cation (their imbalance to be precise) can cause certain tilting or twisting of the octahedra, which may break the inversion symmetry. Here, we substituted a bivalent element into both the B^{+1} and B'^{+3} site in a double perovskite structure $Cs_2BB'X_6$ (X=Cl, Br, I) and studied their effect on the crystal structure, and electronic and optical properties. Although we have simulated a number of compounds $Cs_2BB'X_6$ involving various combinations of B, B', and X (as shown in Table I), let us choose a representative example, Cs_2AgBiX_6 (X= Cl, Br, I), which has been widely studied in the literature. This particular material has been synthesized (except when X= I), and also shown to be chemically stable [13]. Nevertheless, this compound could not stand out as a solar absorber material because of the large value and indirect nature of its band gap. However, when we substituted 25% Pb in place of both Ag^{+1} and Bi^{+3} sites (to balance charge neutrality), not only it reduced the value of band gap but also made it direct in nature. In addition, the transition at the direct band gap is found to be optically allowed, unlike many other compounds of the same class. The drastic effect of Pb substitution can be seen from Fig. 2, which shows the band structure and transition probability (square of dipole transition matrix elements) for $Cs_2AgBiCl_6$ and its Pb-doped counterpart.

Then we went on to simulate the optical properties of this system and found the results to be very interesting. The spectroscopic limited maximum efficiency (SLME) proposed by Yu *et al.* [18] is a well known parameter to quantify the performance of a photovoltaic absorber. The SLME, which takes material specific characteristic properties (band structure, absorption coefficient, etc.) into account while calculating the theoretical efficiency limit, can be seen as an improvement upon the widely known theoretical Shockley-Queisser (S-Q) limit [19] (a detailed discussion about SLME can be found in Ref. [20]). Pb-doped Cs_2AgBiX_6 is found to show high value of absorption coefficients and SLME, comparable to the state of the art hybrid perovskites. Next, we simulated the effect of Pb substitution on a class of possible indirect band gap double perovskites and found a number of promising compounds suitable for solar applications. Few of these compounds turn out to be even more promising than the state of the art lead halide perovskites. One such compound is Pb-doped $Cs_2AgBiBr_6$, which we prepared in our laboratory and measured its electronic properties. The measured structure, magnitude, and direct nature of the band gap confirms our simulated data. Interestingly, this material shows a much higher stability (both against humidity and temperature) than $CH_3NH_3PbI_3$.

The rest of the paper is organized as follows. Details about the crystal structure of the concerned compounds and the primary screening are given in Sec. II. Next, the electronic structure and related discussions are provided in Sec. III. We discuss the optical properties and SLME comparison in Sec IV. Section V is devoted for details of experimental results for Pb-doped $Cs_2AgBiBr_6$. In Sec. VI, we explain the sensitivity of efficiency of these systems to their band gaps along with the conclusion and discussions. The computational and experimental methodology is discussed in Sec. VII.

II. STRUCTURAL DETAILS AND PRIMARY SCREENING

ABX_3 perovskites have a cubic structure where all the B atoms are surrounded by six X atoms forming an octahedron, while A atoms are surrounded by twelve X atoms. For the double perovskites $A_2BB'X_6$, the structure remains similar, with alternate BX_6 and $B'X_6$ octahedra. $A_2BB'X_6$ (X= Cl, Br, I) crystallizes in a cubic structure with space group Fm-$3m$ (No. 225). Here, A occupies the 8c Wyckoff site, B and B' takes the 4a and 4b Wyckoff sites, respectively, while the halide element sits at the 24e site. For halide double perovskites, A and B can be elements having charge state +1, B' are elements with charge state +3, and X are halides (Cl, Br, I) having charge state −1. In the present study, for the parent compounds we

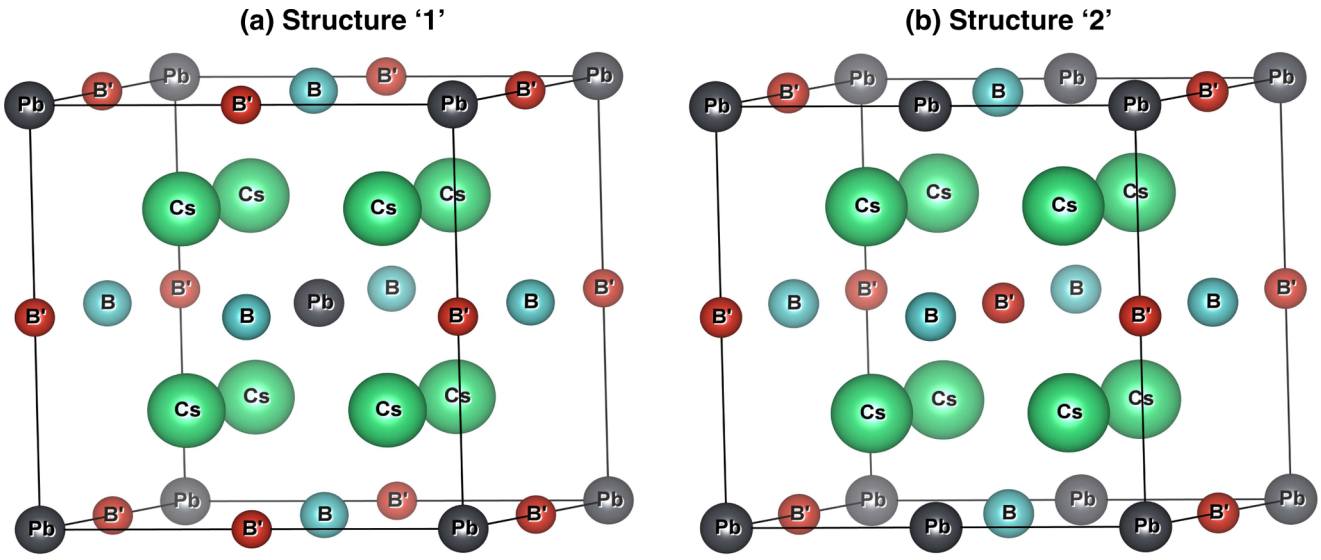

FIG. 1. A conventional unit cell for Pb-doped $Cs_2BB'X_6$. (a) and (b) are the two possible distinct configurations depending on the positions of Pb substituted at B and B' sites. Here, Cs, B, B', and Pb atoms are shown using green, turquoise, red, and grey colored spheres, respectively. Halogen atoms are omitted for convenience.

choose A as Cs, B as G-XI elements (Cu, Ag, Au), and B' as G-XV (Sb, Bi), and G-III (Sc,Y) elements. For these compounds to be stable in the high symmetry cubic structure, two basic tolerance criteria need to be satisfied. The first one is Goldschmidt's tolerance factor $t = (R_A + R_X)/\sqrt{2}(R_B + R_X)$, which should be higher than 0.8 and close to 1. There is another factor called the octahedral factor $\mu(=R_B/R_X)$, which should be larger than 0.414 for BX_6 octahedra to be stable [21]. Here, R_A, R_B, and R_X are the ionic radii of the elements sitting at A, B and B', and X sites, respectively. The first level of screening is done by choosing those parent compounds that satisfy both of these criteria (shown in Table I). The radius of B and B' elements is taken separately, and the tolerance criteria are checked for both octahedra individually. Next, we substitute Pb in these structurally stable parent compounds. Pb, having an ionic radius of 1.19 Å, satisfies the tolerance criteria for all the halides [22].

For the Pb substitution, we took a 40 atom cubic conventional cell for each stable structure consisting of 8 A cations, 4 B cations, 4 B' cations, and 24 X anions. Then one out of each of four B and B' sites are replaced with a Pb atom. In the conventional cell, the B element occupies the positions (in fractional coordinates) (0, 0, 0), (0.0, 0.5, 0.5), (0.5, 0.0, 0.5), and (0.5, 0.5, 0.0) and the B' element occupies the positions (0.5, 0.5, 0.5), (0.5, 0.0, 0.0), (0.0, 0.5, 0.5), and (0.0, 0.0, 0.5). Here we found two possible inequivalent combinations of substitutions. In the first case, we substitute Pb at B (0, 0, 0) and B' (0.5, 0.5, 0.5) sites. In the second case, we put Pb at B (0, 0, 0) and B' (0.5, 0.0, 0.0) sites. These two configurations are shown in Fig. 1. All the other configurations are energetically degenerate to one of these structures and hence are equivalent. We will denote the first structure as structure 1 and the second structure as structure 2 from here onwards.

First-principles calculations were performed by using density functional theory (DFT) [23] with a projector augmented wave (PAW) basis set [24] as implemented in Vienna *ab initio* simulation package (VASP) [25,26]. Pseudopotential formalism with a Perdew-Burke-Ernzerhof (PBE) exchange correlation functional [27] is used to do the primary electronic structure calculations. More accurate estimations of band gaps and other optical properties are carried out using the hybrid Heyd-Scuseria-Ernzerhof (HSE) exchange correlation functional including the spin-orbit coupling (soc). More computational details can be found in the Supplemental Material [20]. Our calculated equilibrium lattice parameters for the well-studied systems $Cs_2AgBiCl_6$ (10.94 Å) and $Cs_2AgBiBr_6$ (11.46 Å) match very well with the previously reported experimental data (10.78 and 11.27 Å) [28]. Small discrepancies in the value can be attributed to the overestimation of the lattice parameter by the GGA exchange-correlation functional, which is a well-known fact. After relaxation, structure 1 retains its cubic symmetry, but structure 2 is found to elongate slightly along the direction where both the parent B and B' elements are replaced by Pb (here x direction). This can be due to the fact that Pb (1.19 Å) has higher atomic radius than all the other B and B' parent elements studied in this work, except for Au (1.37 Å). Even in the case of Au at B site, the average (1.165 Å) for R_B and $R_{B'}$ for the biggest atom Bi (0.96 Å) at B' site is lower than the atomic radius of Pb. This (bigger Pb atom) also accounts for the increased volume of the substituted compounds comparing to the parent compounds. A more detailed discussion on the structural formation based on bond length and electronegativity, along with the theoretically relaxed lattice parameters are reported in Supplemental Material (see Sec. S2 in Ref. [20]).

For a material, chemical stability is a necessary criterion to be satisfied. Here, to determine the chemical stability, we calculate the decomposition enthalpy of the compounds in a possible pathway, namely decomposing to the binary halides of the cations, $A_2PbBB'X_6 \rightarrow AX + PbX_2 + BX + B'X_3$. Details of the quantitative procedure are discussed in the Supplemental Material (Sec. S1 in Ref. [20]). The formation

TABLE II. Relaxed lattice parameters (a, b, c), simulated chemical formation energy (ΔE_F), band gap (E_g), and spectroscopic limited maximum efficiency (SLME) calculated using the hybrid HSE-06 exchange-correlation functional including the effect of spin-orbit coupling (soc) for Pb substituted halide double perovskites. These are the selected list of compounds, which are predicted to be most promising out of a more exhaustive list shown in Ref. [20]. Negative formation energy supports chemical stability of the system. "D" within the parenthesis indicate the direct nature of band gap. SLME ($\eta\%$) is simulated at room temperature ($T = 298$ K), considering a film thickness of 2 μm.

Compound	a (Å)	$b = c$ (Å)	ΔE_F (meV/atom)	E_g(eV) HSE06+soc	SLME ($\eta\%$)
Structure 1 (cubic)					
$Cs_2Pb_{0.5}Ag_{0.75}Bi_{0.75}Cl_6$	11.11		−96.26	1.49(D)	16.31
$Cs_2Pb_{0.5}Ag_{0.75}Sb_{0.75}Cl_6$	11.02		−76.08	1.43(D)	18.55
$Cs_2Pb_{0.5}Au_{0.75}Bi_{0.75}Cl_6$	11.09		−35.52	0.95(D)	23.80
$Cs_2Pb_{0.5}Au_{0.75}Sb_{0.75}Cl_6$	11.01		−18.18	0.94(D)	23.64
$Cs_2Pb_{0.5}Au_{0.75}Sc_{0.75}Cl_6$	10.85		−19.81	2.42(D)	12.38
$Cs_2Pb_{0.5}Au_{0.75}Y_{0.75}Cl_6$	11.03		−8.15	2.45(D)	12.33
$Cs_2Pb_{0.5}Cu_{0.75}Bi_{0.75}Cl_6$	10.89		−61.82	1.03(D)	26.84
$Cs_2Pb_{0.5}Cu_{0.75}Sb_{0.75}Cl_6$	10.82		−41.72	1.09(D)	25.08
$Cs_2Pb_{0.5}Ag_{0.75}Bi_{0.75}Br_6$	11.64		−62.02	1.02(D)	21.01
$Cs_2Pb_{0.5}Au_{0.75}Bi_{0.75}Br_6$	11.61		−11.59	0.54(D)	15.60
$Cs_2Pb_{0.5}Ag_{0.75}Bi_{0.75}I_6$	12.40		−2.46	0.50(D)	16.30
Structure 2 (tetragonal)					
$Cs_2Pb_{0.5}Ag_{0.75}Bi_{0.75}Cl_6$	11.24	11.05	−96.60	1.77(D)	12.30
$Cs_2Pb_{0.5}Ag_{0.75}Sb_{0.75}Cl_6$	11.21	10.96	−75.76	1.78(D)	14.07
$Cs_2Pb_{0.5}Au_{0.75}Sc_{0.75}Cl_6$	11.39	10.69	−18.53	2.28(D)	12.09
$Cs_2Pb_{0.5}Au_{0.75}Y_{0.75}Cl_6$	11.52	10.88	−9.67	2.21(D)	13.05
$Cs_2Pb_{0.5}Cu_{0.75}Bi_{0.75}Cl_6$	11.25	10.77	−62.05	1.13(D)	20.40
$Cs_2Pb_{0.5}Cu_{0.75}Sb_{0.75}Cl_6$	11.24	10.68	−41.82	1.25(D)	16.62
$Cs_2Pb_{0.5}Cu_{0.75}Sc_{0.75}Cl_6$	11.28	10.48	−39.92	2.32(D)	9.27
$Cs_2Pb_{0.5}Cu_{0.75}Y_{0.75}Cl_6$	11.24	10.68	−41.82	2.25(D)	11.25
$Cs_2Pb_{0.5}Ag_{0.75}Bi_{0.75}Br_6$	11.74	11.58	−58.80	1.26(D)	18.52
$Cs_2Pb_{0.5}Ag_{0.75}Bi_{0.75}I_6$	12.50	12.35	−2.62	0.74(D)	20.12

energy (ΔE_F) of the compound from its binary halide salts can be viewed as the reverse physical quantity of the decomposition enthalpy. We have tabulated the simulated data for all the selected compounds, forming in two different structures in Tables 1 and 2, respectively, of Ref. [20]. Here, the negative value indicates the stability of the compound. It is noticeable that for a specific compound, the energetics of structures 1 and 2 are very close (within 1 meV/atom), pointing towards an almost equal probability of formation of the concerned compound in any of these two structures at 25% Pb substitution. This also indicates that disorder can be a common phenomenon in these compounds.

III. ELECTRONIC STRUCTURE

The double perovskites, reported in the literature till date, face two issues. First, some classes have indirect band gap (Cs_2AgBiX_6 being one of them) and the direct gap is at a much higher energy level than the indirect gap. This results in relatively poor absorption (as phonons are required to assist in absorption). Secondly, they suffer from higher possibility of nonradiative recombination loss. These negative facts restrict us from using them as single junction solar cells. By doing a detailed analysis, Savory *et al.* reported that the fundamental mismatch between Ag d and Bi s orbitals is the main reason behind this [29]. They proposed the idea of orbital matching by replacing Ag^{+1} with Tl^{+1} or In^{+1}, which have valence ns^2 electrons in their cationic state, and showed the band gap to become direct. But as discussed earlier, these compounds came out to be thermodynamically unstable [15]. Later, few compounds of the same class (e.g., $Cs_2AgInCl_6$) were reported to show direct nature of band gap [10,11]. But the problem with these compounds was their much large optical band gap. The reason behind this is the presence of inversion symmetry in double perovskite structures, which can result in the bands at VBM and CBM to have same parity, thus making the transition from VBM to CBM optically forbidden [14]. Here we choose Pb, which is known to have very stable +2 oxidation state, and ns^2 ($6s^2$) valence configuration at that cationic state, similar to Bi. Instead of substituting fully (which practically will result in perovskite $CsPbI_3$), we substitute partially at both B and B' sites.

We have calculated the electronic properties [band structure, density of states (DOS), etc.] for all the pure and Pb-substituted compounds using the PBE exchange correlation functional. We assume that for our systems, the shape of the band structure calculated using PBE does not change much compared to others, calculated using more accurate and expensive exchange-correlation functionals. This is usually the case for most of the materials [30,31]. Next, we study the optical properties, where the use of accurate values of the band gap is extremely important. The PBE exchange correlation functional is known to underestimate the band gap value for semiconductors. On the other hand, the Heyd-Scuseria-Ernzerhof (HSE) functional

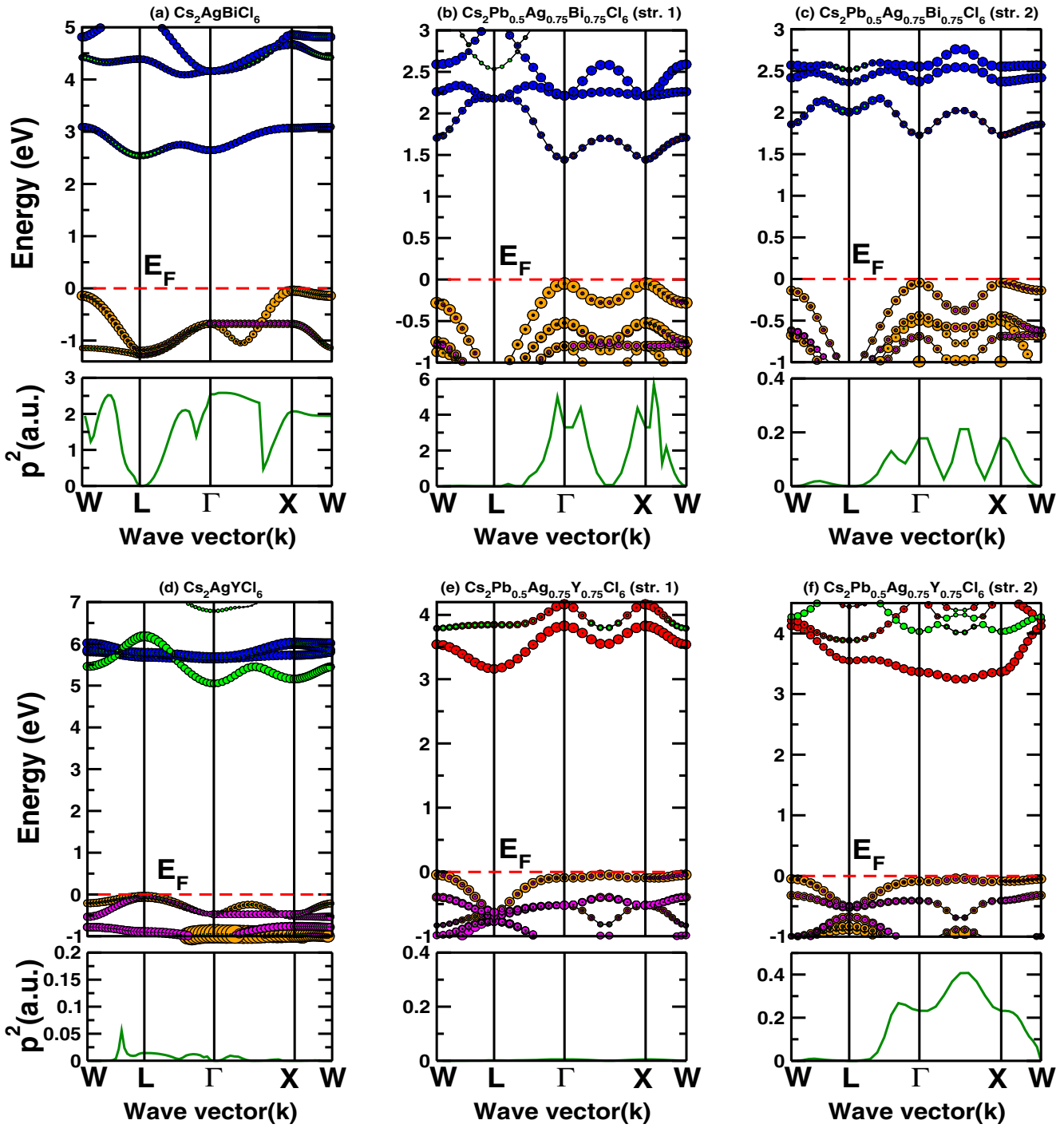

FIG. 2. Band structure (above) and transition probability from VBM to CBM (square of dipole transition matrix elements) (below) for (a) pure $Cs_2AgBiCl_6$ and $Cs_2Pb_{0.5}Ag_{0.75}Bi_{0.75}Cl_6$ in (b) structure 1 and (c) structure 2, respectively. (d)–(f) show similar results but for Cs_2AgYCl_6. All the calculations are done using PBE exchange-correlation functional including spin-orbit coupling (soc) effect. In these plots, band gaps are rigidly shifted to the HSE06+soc calculated values for convenience. All the energies are plotted taking valence band maxima as zero. Here, Cl-p, Ag-d, B'-p (when B'=Bi) or B'-d (when B'=Y), Ag-s, and Pb-p states are shown in orange, magenta, blue, green, and red colored circles, respectively.

is seen to predict the band gap quite close to the experiment. The spin-orbit coupling (soc) has great effect on the electronic properties of these class of systems. We have included soc in all our calculations. As such, primarily we did the electronic structure calculation using PBE+soc, whereas, accurate value of the band gap is calculated using HSE06+soc exchange correlation functional (validation and more details of the computational procedure can be found in the Supplemental Material) [20]. PBE+soc band structure with the relatively more accurate band gap obtained using HSE06+soc exchange correlation functional, is then used for further optical calculations.

We choose to screen a large number of parent compounds ($Cs_2BB'X_6$, X=Cl, Br, I), with a permutation of group (G)-XI elements (Cu, Ag, Au) at B site and G-XV(Sb,Bi) and G-III(Sc,Y) elements at B' site and hence examine the effect of Pb substitution. All these compounds show indirect band gap in the parent state. With small Pb substitution, most of them transform to a direct band gap (see Tables 1 and 2 of Ref. [20]). In order to get a deeper insight, we have calculated the orbital projected density of states (DOS) for the pure and Pb-substituted systems. We particularly choose two systems, $Cs_2AgBiCl_6$ and Cs_2AgYCl_6 and their Pb-substituted counterpart, to analyze their electronic properties in this paper. These two systems can be seen as representatives of their respective classes. We have provided all the electronic structure data (band structure, orbital projected density of states, etc.) for the rest of the possible compounds in the Supplemental Material (see Sec. S3 in Ref. [20]).

Pure $Cs_2AgBiCl_6$ is an indirect band gap material having valence band maxima (VBM) and conduction band minima (CBM) at X and L high-symmetry points in reciprocal space as shown in Fig. 2(a). Detailed analysis of orbital projected DOS (shown in Ref. [20]) shows that it has Ag 4d/Cl 3p, Bi 6s/Cl 3p character in the VBM and Ag 5s/Cl 3p, Bi 6p/Cl 3p antibonding character in CBM. It has been reported that Ag 4d and Bi 6s interaction pushes the valence band to higher energy at X point leading to indirect nature of the band gap [29]. With Pb substitution, two different scenarios arise for structures 1 and 2. Using the orbital projected density of states, we tried to draw a qualitative molecular orbital diagram for $Cs_2Pb_{0.5}Ag_{0.75}Bi_{0.75}Cl_6$ as shown in Fig. 3(a). Pb, having higher energy 6s atomic orbitals, contributes to the valence band pushing it higher than in the parent compound, at Γ and X points. It can be clearly seen from the orbital projected DOS that VBM is mainly composed of Ag 4d/Cl 3p and Pb 6s/Cl 3p antibonding orbitals. Spin-orbit coupling plays an integral role in the electronic structure of these systems, especially for structure 2. Inclusion of spin-orbit coupling splits the Bi and Pb p orbitals, which results in lowering of the conduction band mainly at Γ and X points, as can be seen from Fig. 2. This causes both structures 1 and 2 to have a direct nature of band gap. The band structure and DOS for other Pb-substituted compounds in this family, i.e., Cs_2(Cu, Ag, Au)(Sb, Bi)X_6 are shown in the Supplemental Material [20]. In case of Sb at B' site, the band gap remains similar, only the conduction bandwidth decreases, which can be attributed to a smaller spread of Sb $p_{3/2}$ and Sb $p_{1/2}$ orbitals compared to Bi p orbitals. In the compounds with Cu at B site, the band gap reduces significantly comparing to its Ag counterpart, which can be attributed to Cu d orbitals having higher energy than Ag d orbitals, which pushes the valence band even higher. Au having significantly higher electronegativity (2.64) than both Ag (1.93) and Cu (1.9), have the Au-s atomic orbitals lower in energy than the other two. This affects in lowering the conduction band energy at L point, making it indirect for both structures 1 and 2. The effect of spin-orbit coupling changes the nature of band gap from indirect to direct for structure 1 but structure 2 remains indirect in nature. In all the cases, changing the halide from Cl → Br → I, lifts the VBM as the atomic p-orbital energy increases with decreasing electronegativity (with increasing atomic number in halides). The valence bandwidth decreases as the difference in energy between B d and X p orbitals decreases. Due to the stronger delocalization of p orbitals going from Cl → Br → I, the bottom of the conduction band widens. These changes result in a lower band gap from chlorides to iodides.

Cs_2AgYCl_6 belong to another class. The band structure for this representative compound is shown in Fig. 2(d). For this compound, the VBM is at L point and is mainly composed of Ag 4d/Cl 3p antibonding character. CBM mainly comprises Ag 5s/Cl 3p orbitals at Γ. It also has Y 4d/Cl 3p antibonding character. The bonding characteristics for Y 4d/Cl 3p orbitals can be seen 2–3 eV lower than the VBM. Pb substitution introduces Pb 6s states in the valence band pushing it to higher energy in the middle of Γ and X, causing a reduction in the band gap. Here, for structure 1, CBM is at L point resulting in indirect nature of band gap. However, for structure 2, next nearest Pb 6p,Pb 6p/Cl 3p interaction is seen to drag down the CBM in the middle of Γ-X line, making the band gap direct. The band structure and DOS for other Pb-substituted compounds in this family, i.e., Cs_2(Cu, Ag, Au)(Sc, Y)X_6 are shown in Ref. [20]. Sc having higher electronegativity than Y has Sc 3d atomic orbitals lower in energy than Y. But this energy difference is very small leading to almost similar band gaps. In the case of Cu, the band pattern remains similar to Ag, giving a direct band gap for structure 2, but reduces the gap significantly. Structure 1 becomes direct in case of Au incorporation at B site, showing a direct gap in the middle of Γ and X and W point. This again can be attributed to much higher electronegativity of Au leading to a significantly lower Au-s atomic orbital than both Ag and Cu. Au in structure 2 is seen to have a direct gap similar to Ag and Cu. For chlorides, the band gap for these class of compounds remains in the higher visible side. However, changing the halide from Cl → Br → I reduces the gap, putting it well in the visible region.

For comparison sake, simulated data for band gap (magnitude and nature) with different exchange correlation functionals and decomposition enthalpies for all the systems are reported in Tables 1 and 2 of Ref. [20]. It can be seen that Pb substitution decreases the band gap considerably for a number of these systems, taking it well into the visible region. However, there are still few systems which are either indirect or unstable (+ve formation enthalpy). At this stage, we shortlist only those compounds that have direct band gap and are stable to perform further investigation of optical absorption and device efficiency. The list of these selected compounds (in both structures 1 and 2) is shown in Table II.

IV. OPTICAL ABSORPTION COEFFICIENT AND SPECTROSCOPIC LIMITED MAXIMUM EFFICIENCY (SLME)

Hybrid halide perovskites have taken the solar cell development to a new level by showing rapid growth in efficiency. This is attributed to its excellent absorption ability and long carrier diffusion length. Careful analysis of the electronic structure reveals that the reason for the strong absorption is the direct p-p transition from valence band (consisting of a halide p orbital) to the conduction band (consisting of Pb p) [32]. The compounds we have discussed so far also show direct p-p transition form VBM to CBM. This motivates us to proceed

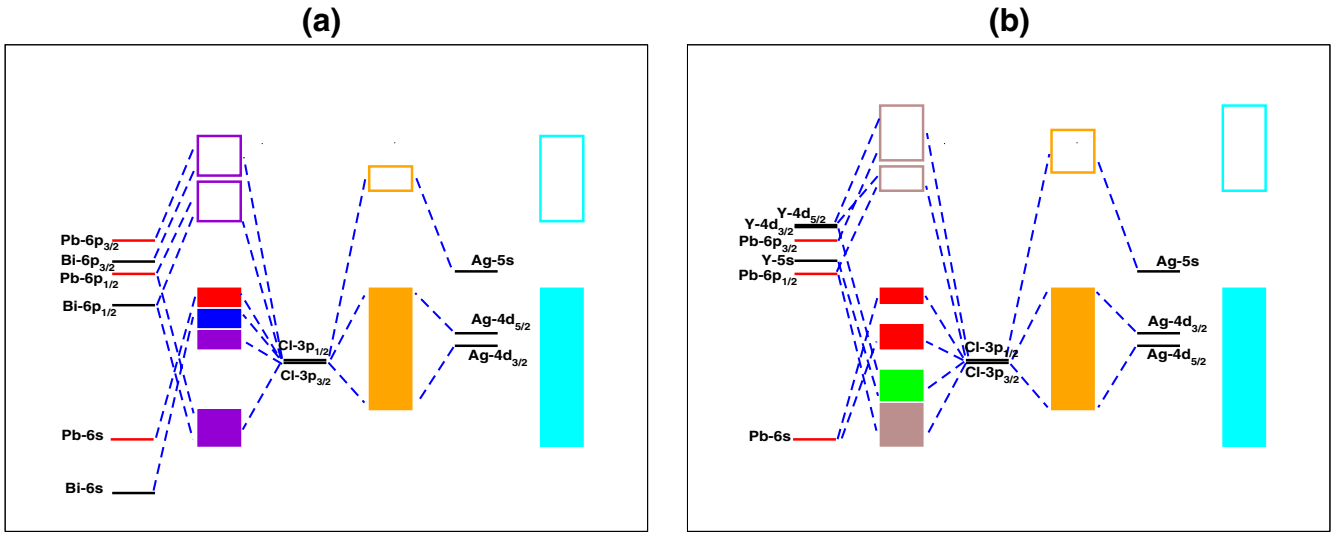

FIG. 3. Molecular orbital diagram for Pb-doped (a) $Cs_2AgBiCl_6$ and (b) Cs_2AgYCl_6. Atomic orbitals for Ag, Bi, Y, and Cl are marked with black lines and for Pb they are red. Empty boxes signify unfilled conduction bands, whereas filled ones represent valence bands. In (a), red colored bands signify contribution from Pb and Cl only. Blue signifies Bi-Cl interaction, and mixed Bi-Cl, Pb-Cl bands are marked in violet color. In (b), red colored bands signify contribution from Pb and Cl only. Green signifies Y-Cl interaction, and mixed Y-Cl, Pb-Cl bands are shown in brown color. Ag-Cl bands are marked in orange color in both of the figures. Atomic orbital energies are taken from (http://www.nist.gov). Molecular orbitals are drawn by looking at the orbital projected density of states for these systems (can be found in Ref. [20]).

further and study the necessary optical properties of these systems to be considered as solar absorbers. Here we choose a parameter known as a spectroscopic limited maximum efficiency (SLME) introduced by Yu *et al.* [18] as a screening parameter. SLME gives the maximum possible solar power conversion efficiency incorporating the nature of the band gap and absorption coefficient for a particular compound. This can be seen as necessary improvement upon the Shockley-Queisser (S-Q) efficiency parameter (more details about SLME and related parameters can be found in Ref. [20]).

As discussed above, SLME includes two material specific properties. First, it is the nature of the band gap. For various double perovskites, even after acquiring a direct electronic band gap, it is seen that the optical transition from VBM to CBM was forbidden. This arises because VBM and CBM turn out to have same parity, due to the inversion symmetry present in these structures. In order to check the possibility of optical transition from VBM to CBM for our systems, we have calculated the dipole transition matrix elements, the square of which can essentially be seen as the probability of transition. We have plotted the square of the dipole transition matrix elements (p^2) for all the systems (below their respective band structure plots) as shown in Fig. 2 of this paper and Sec. S3 of Ref. [20]. It is clear that the transition from VBM to CBM at the direct electronic band gap is allowed (for most of the systems), encouraging us to proceed further with the calculation of the next relevant properties, namely the absorption coefficient (α) and SLME.

The absorption coefficient (α) for a material can be seen as a quantifiable parameter which basically shows how deep a photon with a particular wavelength can penetrate into the material before it is absorbed. For semiconductors, as the photons below the energy of the band gap take almost no part in absorption, a sharp rise in the absorption coefficient is expected after a threshold incident photon energy close to its band gap. For a semiconducting material, the absorption coefficient (α) is directly related to its dielectric function by the following equation:

$$\alpha(E) = \frac{2\omega}{c}\sqrt{\frac{\sqrt{\epsilon_{re}^2 + \epsilon_{im}{}^2} - \epsilon_{re}}{2}}. \quad (1)$$

Here, E is the incident photon energy, ω is the angular frequency related to E, by $E = \hbar\omega$, $\hbar$ is the reduced Planck's constant, and c is the speed of light in vacuum. ϵ_{re} and ϵ_{im} are the real and imaginary parts of dielectric function at that energy. Equation (1) is a simplified version, showing α as scalar. Actually, α and the related ϵ's are second-rank tensors. Here, we used density functional theory under the independent particle approximation to calculate the frequency (energy) dependent dielectric function. Other necessary details and validation of the calculations can be found in Ref. [20].

The optical absorption coefficient for all the selected systems (as in Table II) is plotted in Figs. 4(a) (for structure 1) and 4(c) (for structure 2). For comparison sake, we have also plotted the absorption coefficient for $CH_3NH_3PbI_3$ and its inorganic counterpart $CsPbI_3$. From the figures, it can be seen that some of the systems have an absorption coefficient (α) comparable to $CH_3NH_3PbI_3$. Also, few systems with a band gap lower than $CH_3NH_3PbI_3$ will be able to cover the solar spectrum near the reddish side. Next, we calculated the thickness dependent SLME for all these systems. Figures 4(b) and 4(d) show the SLME versus film thickness for our selected systems in two possible structures, respectively. Here also, we have plotted similar data for $CH_3NH_3PbI_3$ and $CsPbI_3$, to see how our systems trade with the state of the art scenario. Interestingly, one can see that few of our proposed materials have SLME comparable to the state of the art $CH_3NH_3PbI_3$. Even more

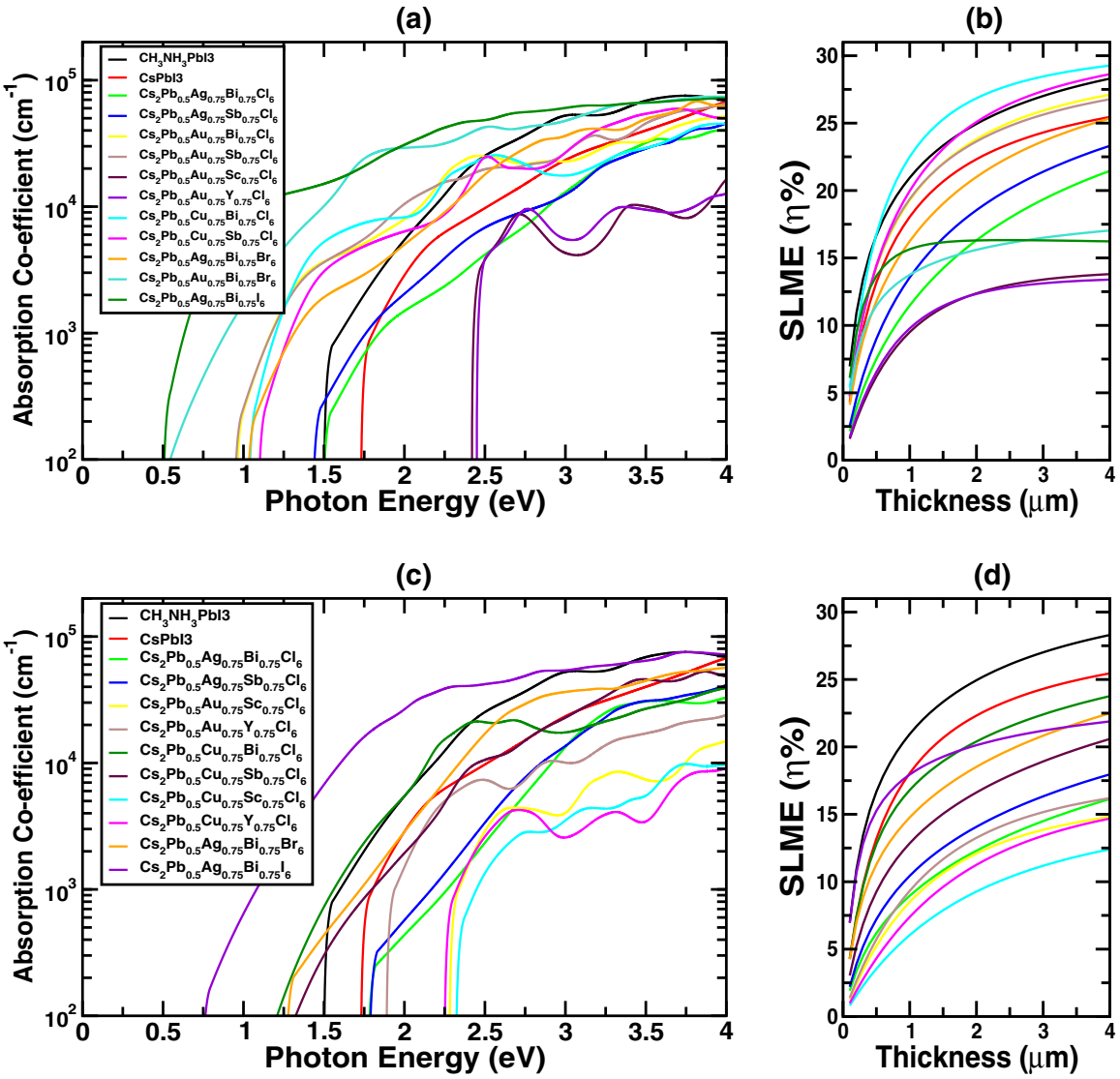

FIG. 4. (a) and (c) Absorption coefficient vs incident photon energy and (b) and (d) spectroscopic limited maximum efficiency vs film thickness at 298 K for various compounds (as in Table II) in structures 1 and 2, respectively. For comparison, simulated results for $CH_3NH_3PbI_3$ and its inorganic counterpart $CsPbI_3$ are also given.

remarkable are few systems (Cu-based) with even higher efficiency than $CH_3NH_3PbI_3$. These excellent SLME can essentially be attributed to a very high absorption coefficient and having band gaps well in the visible region and very near to the ideal S-Q region.

For completeness, we have also tabulated the room temperature (298 K) simulated value of few important device parameters, such as short-circuit current density (J_{sc}), open-circuit voltage (V_{oc}), current density (J_{max}) and voltage (V_{max}) at maximum power output, and fill factor (FF) at film thickness 2 μm (see Tables 3 and 4 in Ref. [20]).

V. EXPERIMENTAL RESULTS

Solution deposition techniques used to prepare the parent and the Pb-substituted $Cs_2AgBiBr_6$. $CsPbBr_3$ is also prepared for comparative analysis. X-ray diffraction measurement was carried out to confirm the phase purity and hence stability of these compounds. Figure 5(a) shows the powder pattern obtained for both the parent compounds $CsPbBr_3$ and $Cs_2AgBiBr_6$. $Cs_2AgBiBr_6$ crystallizes in 3D double perovskite structure, in cubic Fm-3m space group with a unit cell parameter of $a = 11.27$ Å [28], which compares fairly well with the simulated value. Doping of $Cs_2AgBiBr_6$ with $CsPbBr_3$ was carried out, by mixing the two solutions in appropriate ratios. The powder diffraction pattern of Pb-doped $Cs_2AgBiBr_6$ is also shown in Fig. 5(a) (red curve). As obvious from the powder pattern, $Cs_2Pb_{0.5}Ag_{0.75}Bi_{0.75}Br_6$ retain the original double perovskite structure.

The band gap of the pristine and the Pb-substituted films were determined using UV-Vis absorption spectroscopy. Figure 5(b) shows the absorption spectra obtained for the pristine and the Pb^{2+} substituted films. The spectra show a steep onset at around 550 nm for $Cs_2AgBiBr_6$ and a redshift of 30 nm (absorption onset around 580 nm) was observed for $Cs_2Pb_{0.5}Ag_{0.75}Bi_{0.75}Br_6$. From the Tauc plots, direct band gaps

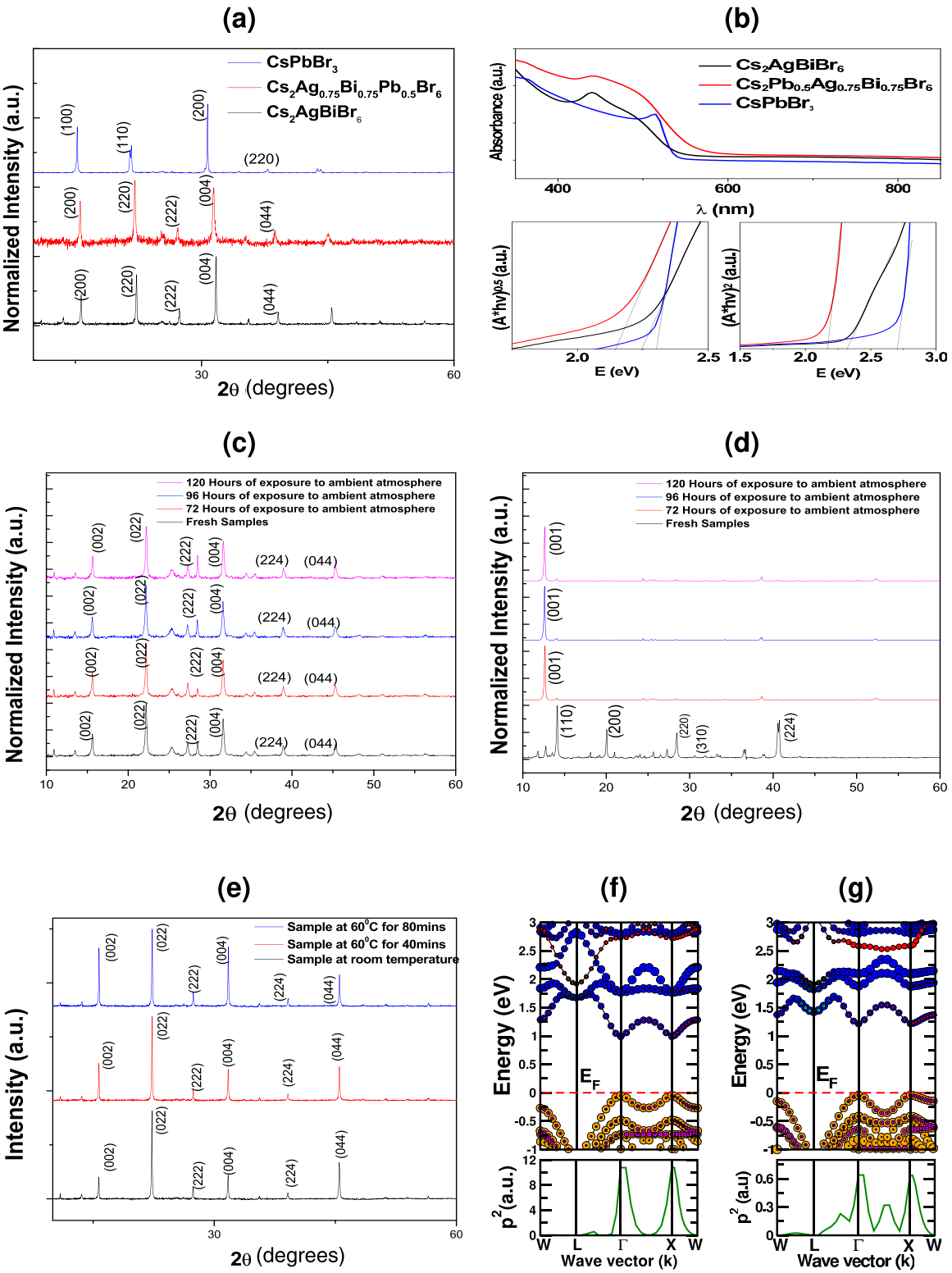

FIG. 5. (a) Stacked XRD pattern and (b) UV-visible plot for $CsPbBr_3$, $Cs_2Pb_{0.5}Ag_{0.75}Bi_{0.75}Br_6$, and $Cs_2AgBiBr_6$. (b) also includes the Tauc plots for the aforementioned compounds. Stacked XRD pattern for (c) $Cs_2Pb_{0.5}Ag_{0.75}Bi_{0.75}Br_6$ and (d) $CH_3NH_3PbI_3$ showing behavior in humid atmospheric conditions, and (e) stacked XRD pattern showing thermal stability for $Cs_2Pb_{0.5}Ag_{0.75}Bi_{0.75}Br_6$. The band structure (band gaps scissor shifted to HSE06+soc values) (above) and transition probability from VBM to CBM (square of dipole transition matrix elements) (below) for $Cs_2Pb_{0.5}Ag_{0.75}Bi_{0.75}Br_6$ in (f) structure 1 and (g) structure 2.

of 2.31, 2.13, and 2.69 eV were observed for $Cs_2AgBiBr_6$, $Cs_2Pb_{0.5}Ag_{0.75}Bi_{0.75}Br_6$, and $CsPbBr_3$, respectively. Their respective indirect band gaps were 2.21, 2.10, and 2.27 eV. Substitution by Pb^{2+} resulted in a decrease in the band gap of both the parent compounds. It can be observed that, although the indirect band gaps for the parent compounds are significantly lower than their respective direct band gaps, the direct and indirect band gap of the Pb-doped compound is almost the same. This, in turn, supports our theoretical findings suggesting indirect to direct band gap transition. We have plotted the band structure of $Cs_2Pb_{0.5}Ag_{0.75}Bi_{0.75}Br_6$, for both structures 1 and 2 in Figs. 5(f) and 5(g), respectively, for a one-to-one comparison with the experimental results. From the band structures it is clear that $Cs_2Pb_{0.5}Ag_{0.75}Bi_{0.75}Br_6$ has direct nature of band gap in both the structures (1 and 2), confirming an indirect to direct transition when Pb is substituted in $Cs_2AgBiBr_6$. Although, the magnitude of the band gap does not exactly match with the measured values, the red shift of the band gap from both $Cs_2AgBiBr_6$ and $CsPbBr_3$ is visible here.

The structural stability of the double perovskite has to be evaluated in order for them to be considered feasible for application in solar cells. In order to study the stability of the material, Pb^{2+}-doped double perovskite films were exposed to ambient atmosphere for a period of 120 h with humidity of about 55% on average. For comparison sake, we have also checked the stability of $CH_3NH_3PbI_3$ under exactly the same atmospheric conditions. Powder diffraction analysis was carried out periodically and the results obtained are shown in Figs. 5(c) and 5(d) for $Cs_2Pb_{0.5}Ag_{0.75}Bi_{0.75}Br_6$ and $CH_3NH_3PbI_3$, respectively. It can be seen that even after 120 h of full exposure to highly humid conditions, the powder patterns remain the same for the former, confirming the robust stability of the material against atmospheric conditions, while $CH_3NH_3PbI_3$ degrades to a binary lead halide after 72 hours, as obvious from the powder diffraction pattern.

The stability of Pb-doped double perovskite films were also checked against extreme thermal conditions by exposing the sample to continuous heating at 65 deg C for 80 minutes and periodically checking the XRD patterns. The powder patterns at different time intervals are shown in Fig. 5(e). The patterns show no significant change in the reflections from the XRD analysis, indicating good thermal stability with respect to temperature. Thus $Cs_2Pb_{0.5}Ag_{0.75}Bi_{0.75}Br_6$ acquires robust atmospheric as well as thermal stability along with promising optical absorption properties, making it a promising candidate for potential solar cell materials, even better than the state of the art $CH_3NH_3PbI_3$.

VI. CONCLUSION AND DISCUSSION

In conclusion, we propose a class of brand new materials which, due to their better efficiency, stability, and minimal toxicity, can substitute the state of the art photovoltaic absorber material $CH_3NH_3PbI_3$ for solar cell applications. These new compounds are double perovskite materials ($Cs_2BB'X_6$) doped with a small amount of lead. Pb^{+2} doping at both B and B' sites shows three major positive effects: (i) helps to achieve indirect-direct band gap transition via orbital matching, (ii) pushes the valence band higher, resulting in a significant reduction in the band gap, and (iii) introduces some new bands at CBM with different parity making possible the optical transition between VBM to CBM. We have also calculated the optical absorption spectra of these systems and found a very high absorption coefficient, comparable (sometimes higher) to the state of the art material $MAPbI_3$. The solar efficiency (SLME) calculation on these systems reveals quite high efficiencies for a number of compounds. The calculation of decomposition enthalpy indicates toward stability against possible degradation to binary halides. Apart from simulation, one of the proposed materials, $Cs_2Pb_{0.5}Ag_{0.75}Bi_{0.75}Br_6$, is prepared in our laboratory and its stability and electronic properties are discussed in detail. Our theoretical results match fairly well with the experimental data, confirming the validity of other theoretically predicted materials. A one-to-one comparison of the measured stability of this particular compound with those of $MAPb_3$ shows the former to be much superior: a bottleneck for the later, which remains a major concern in the photovoltaic community.

A. Further ideas to improve the efficiency of proposed materials

Substituting the inorganic Cs element with CH_3NH_3 or other organic cations may push the efficiency limit even further and make them more stable. Lead halide perovskites have been the center of attention of the photovoltaic research community for quite some time, while still having issues with toxicity and stability. Our proposal is a breakthrough to address these concerns and achieve potentially solar efficient materials at 75% less toxicity and much higher stability.

It is well known that the solar efficiency of a device is quite sensitive to the actual value of the band gap of the material used. As there are no experimental band gap data available for these newly proposed materials, we have checked the sensitivity of the SLME with its band gap value. (Details of the procedure can be found in Ref. [20].) We have tabulated the SLME for these systems at $\pm 10\%$ of their HSE06+soc band gap in Table III. We have also calculated the ideal band gap for each system at which SLME is maximum, as shown in the last two columns. Notably, the ideal band gap falls in the region of 1.0–1.2 eV. In fact, some of the compounds [$Cs_2Pb_{0.5}(Cu,Au)_{0.75}(Bi,Sb)_{0.75}Cl_6$, $Cs_2Pb_{0.5}Ag_{0.75}Bi_{0.75}Br_6$] show very high efficiencies, as much as $\sim$31.5%. From Figs. 4(a) and 4(c), it can be seen that $Cs_2Pb_{0.5}Ag_{0.75}Bi_{0.75}I_6$ has excellent absorption spectra (higher than others), but with a low band gap. This significantly reduces the simulated attainable voltage, reducing the efficiency. However, it has a potential to reach very high efficiency, by making the band gap slightly higher (see Table III). This can be thought to be achieved via lowering the Pb substitution percentage. On the other hand, chloride compounds with G-III (Sc,Y) at B' sites, show very high band gaps (significantly adrift of the ideal region), resulting in poor SLME. The band gap for such systems reduces by changing the halide from chloride to iodide, which again can boost the performance.

VII. METHODS

A. Computational methodology

First-principles calculations were performed using density functional theory (DFT) [23] as implemented in Vienna

TABLE III. Sensitivity of SLME ($\eta\%$) with band gap for Pb substituted double perovskites (structures 1and 2). E_g is the calculated band gap E_g using HSE+soc. We also tabulated the ideal band gap at which the calculated SLME is maximum, as shown in the last two columns. SLME ($\eta\%$) is simulated at room temperature ($T = 298$ K), considering a film thickness of 2 μm.

Compound	E_g(eV) (HSE06+soc)	($\eta\%$) (E_g)	($\eta\%$) (E_g+10%)	($\eta\%$) (E_g−10%)	($\eta\%$) max.	E_g(eV) $(\eta\%)_{max}$
Structure 1 (cubic)						
$Cs_2Pb_{0.5}Ag_{0.75}Bi_{0.75}Cl_6$	1.49	16.31	14.53	17.82	19.05	1.10
$Cs_2Pb_{0.5}Ag_{0.75}Sb_{0.75}Cl_6$	1.43	18.55	16.87	19.77	20.67	1.11
$Cs_2Pb_{0.5}Au_{0.75}Bi_{0.75}Cl_6$	0.95	23.80	24.25	22.84	24.37	1.11
$Cs_2Pb_{0.5}Au_{0.75}Sb_{0.75}Cl_6$	0.94	23.64	24.08	22.77	24.24	1.11
$Cs_2Pb_{0.5}Au_{0.75}Sc_{0.75}Cl_6$	2.42	12.38	8.30	16.69	30.51	1.16
$Cs_2Pb_{0.5}Au_{0.75}Y_{0.75}Cl_6$	2.45	12.33	8.00	17.22	31.53	1.16
$Cs_2Pb_{0.5}Cu_{0.75}Bi_{0.75}Cl_6$	1.03	26.84	27.15	26.13	27.15	1.13
$Cs_2Pb_{0.5}Cu_{0.75}Sb_{0.75}Cl_6$	1.09	25.08	24.93	24.67	25.13	1.12
$Cs_2Pb_{0.5}Ag_{0.75}Bi_{0.75}Br_6$	1.02	21.01	21.07	20.61	21.08	1.11
$Cs_2Pb_{0.5}Au_{0.75}Bi_{0.75}Br_6$	0.54	15.60	16.49	14.59	19.19	0.93
$Cs_2Pb_{0.5}Ag_{0.75}Bi_{0.75}I_6$	0.50	16.30	18.14	14.30	29.07	1.14
Structure 2 (tetragonal)						
$Cs_2Pb_{0.5}Ag_{0.75}Bi_{0.75}Cl_6$	1.77	12.30	9.91	14.58	18.64	1.03
$Cs_2Pb_{0.5}Ag_{0.75}Sb_{0.75}Cl_6$	1.78	14.07	11.47	16.54	20.74	1.11
$Cs_2Pb_{0.5}Au_{0.75}Sc_{0.75}Cl_6$	2.28	12.09	8.52	15.99	27.25	1.16
$Cs_2Pb_{0.5}Au_{0.75}Y_{0.75}Cl_6$	2.21	13.25	9.76	17.00	27.02	1.16
$Cs_2Pb_{0.5}Cu_{0.75}Bi_{0.75}Cl_6$	1.13	20.40	19.73	20.62	20.62	1.02
$Cs_2Pb_{0.5}Cu_{0.75}Sb_{0.75}Cl_6$	1.25	16.62	15.52	17.40	17.65	0.99
$Cs_2Pb_{0.5}Cu_{0.75}Sc_{0.75}Cl_6$	2.32	9.27	6.27	12.62	23.82	1.12
$Cs_2Pb_{0.5}Cu_{0.75}Y_{0.75}Cl_6$	2.25	11.25	7.99	14.70	24.28	1.13
$Cs_2Pb_{0.5}Ag_{0.75}Bi_{0.75}Br_6$	1.26	18.52	17.47	19.26	19.37	1.03
$Cs_2Pb_{0.5}Ag_{0.75}Bi_{0.75}I_6$	0.74	20.12	21.15	18.80	22.78	1.08

ab initio simulation package (VASP) [25,26]. Finding the equilibrium structures and the calculation of decomposition enthalpy and other primary electronic structure characteristics (band structure, density of states, etc.) were done using the Perdew-Burke-Ernzerhof (PBE) exchange correlation functional [27]. Next, accurate values of the direct band gaps were calculated using the Heyd-Scuseria-Ernzerhof (HSE06) functional [33] taking the band edge information from the PBE calculated band structures. Spin-orbit coupling has been included in all the calculations. More details and validation of the procedure have been discussed in Ref. [20]. The optical absorption coefficients are calculated within the independent particle approximation with a PBE exchange correlation functional and then a scissor shifted to the HSE06 obtained band gap while calculating the SLME. Again, more details about the procedure and validation can be found in Ref. [20].

B. Experimental synthesis

All chemicals used were from Sigma Aldrich 99.99% pure anhydrous grade. A solution in DMSO containing 0.5 mM equivalent of CsBr (106 mg) and 0.25 mM each of AgBr (47 mg) and $BiBr_3$ (112.5 mg) was prepared. This was used as the parent solution for the preparation of pure $Cs_2AgBiBr_6$ films. Another solution was prepared containing 0.5 mM each of CsBr (106 mg) and $PbBr_2$ (183.5 mg). This solutions was mixed in appropriate ratios with the parent solution to obtain different percentage of lead doping. $Cs_2AgBiBr_6$ and $Cs_2Pb_{0.5}Ag_{0.75}Bi_{0.75}Br_6$ films were formed on plain glass slides coated with mesoporous TiO_2 following the procedure followed in Ref. [34]. Mesoporous TiO_2 solution was prepared by taking 1:3.5 weight ratio of DyeSol 17.5 NRT TiO_2 paste and ethanol, and stirring for around 2 h. The solution was spin coated on plain glass slides at 3500 rpm for 30 seconds and sintered at 500 deg C for 15 minutes. The active layers were formed by spin coating warm perovskite solutions (heated at 70 deg C) at 200 rpm for 25 s on the substrates (also heated at 70 deg C) and annealing at 270 deg C for 10 min. In order to synthesize methyl ammonium iodide, a solution of 33% methylamine in ethanol was taken in a round bottom flask and an equimolar amount of 57% hydroiodic acid (HI) was added drop wise to the vigorously stirring solution, maintained at 0 deg C, and further stirred for 2 h. The solvent was then evaporated under reduced pressure to obtain white crystalline methylammonium iodide (CH_3NH_3I) powder. The powder was washed thrice with diethyl ether to remove the excess HI and dried in vacuum oven overnight at 50 deg C. In order to prepare a solution for making $CH_3NH_3PbI_3$ films, equimolar (1 mM each) amounts of CH_3NH_3I and PbI_2 were taken in 1 ml DMSO and spin coated at 3000 rpm for 30 s on substrates coated with mesoporous TiO_2 and annealed at 100 deg C for 10 minutes. The UV-Visible spectroscopy was done using PerkinElmer LAMBDA 750 to study the optical properties, and x-ray diffraction was done using Philips PW1830 x-ray diffraction spectrometer x-ray diffractometer (XRD) to study the structural behavior of the materials under exposure to ambient air and temperature over a period of time [35–37].

ACKNOWLEDGMENTS

J.K. acknowledges financial support from IIT Bombay in the form of a Teaching Assistantship. A.A. and A.Ye. acknowledges National Center for Photovoltaic Research and Education (NCPRE), IIT Bombay for possible funding to support this research. VS thanks DST-INSPIRE fellowship for the financial support and this research activity is partly supported by Department of Science and Technology, Government of India under Grant No. DST/TMD/SERI/S111(G).

[1] A. Kojima, K. Teshima, Y. Shirai, and T. Miyasaka, J. Am. Chem. Soc. **131**, 6050 (2009).
[2] J. Qian, B. Xu, and W. Tian, Org. Electron. **37**, 61 (2016).
[3] W.-J. Yin, J.-H. Yang, J. Kang, Y. Yan, and S.-H. Wei, J. Mater. Chem. A **3**, 8926 (2015).
[4] L. A. Frolova, D. V. Anokhin, K. L. Gerasimov, N. N. Dremova, and P. A. Troshin, J. Phys. Chem. Lett. **7**, 4353 (2016).
[5] A. Kumar, K. R. Balasubramaniam, J. Kangsabanik, Vikram, and A. Alam, Phys. Rev. B **94**, 180105(R) (2016).
[6] N. K. Noel, S. D. Stranks, A. Abate, C. Wehrenfennig, S. Guarnera, A.-A. Haghighirad, A. Sadhanala, G. E. Eperon, S. K. Pathak, M. B. Johnston *et al.*, Energy Env. Sci. **7**, 3061 (2014).
[7] T. Yokoyama, D. H. Cao, C. C. Stoumpos, T.-B. Song, Y. Sato, S. Aramaki, and M. G. Kanatzidis, J. Phys. Chem. Lett. **7**, 776 (2016).
[8] G. Volonakis, M. R. Filip, A. A. Haghighirad, N. Sakai, B. Wenger, H. J. Snaith, and F. Giustino, J. Phys. Chem. Lett **7**, 1254 (2016).
[9] A. H. Slavney, T. Hu, A. M. Lindenberg, and H. I. Karunadasa, J. Am. Chem. Soc. **138**, 2138 (2016).
[10] G. Volonakis, A. A. Haghighirad, R. L. Milot, W. H. Sio, M. R. Filip, B. Wenger, M. B. Johnston, L. M. Herz, H. J. Snaith, and F. Giustino, J. Phys. Chem. Lett. **8**, 772 (2017).
[11] A. Jain, O. Voznyy, and E. H. Sargent, J. Phys. Chem. C **121**, 7183 (2017).
[12] S. Chakraborty, W. Xie, N. Mathews, M. Sherburne, R. Ahuja, M. Asta, and S. G. Mhaisalkar, ACS Energy Lett. **2**, 837 (2017).
[13] X.-G. Zhao, J.-H. Yang, Y. Fu, D. Yang, Q. Xu, L. Yu, S.-H. Wei, and L. Zhang, J. Am. Chem. Soc. **139**, 2630 (2017).
[14] W. Meng, X. Wang, Z. Xiao, J. Wang, D. B. Mitzi, and Y. Yan, J. Phys. Chem. Lett. **8**, 2999 (2017).
[15] Z. Xiao, K.-Z. Du, W. Meng, J. Wang, D. B. Mitzi, and Y. Yan, J. Am. Chem. Soc. **139**, 6054 (2017).
[16] T. T. Tran, J. R. Panella, J. R. Chamorro, J. R. Morey, and T. M. McQueen, Mater. Horiz. **4**, 688 (2017).
[17] A. H. Slavney, L. Leppert, D. Bartesaghi, A. Gold-Parker, M. F. Toney, T. J. Savenije, J. B. Neaton, and H. I. Karunadasa, J. Am. Chem. Soc. **139**, 5015 (2017).
[18] L. Yu and A. Zunger, Phys. Rev. Lett. **108**, 068701 (2012).
[19] W. Shockley and H. J. Queisser, J. Appl. Phys. **32**, 510 (1961).
[20] See Supplemental Material at http://link.aps.org/supplemental/10.1103/PhysRevMaterials.2.055401 in which a brief formalism for calculating the dielectric constants is given in Sec. S1 C, which includes Ref. [35]. In Sec. S1 D, brief discussion about SLME can be found which includes Refs. [36,37].
[21] C. Li, X. Lu, W. Ding, L. Feng, Y. Gao, and Z. Guo, Acta Crystallogr., Sect. B: Struct. Sci. **64**, 702 (2008).
[22] R. T. Shannon and C. T. Prewitt, Acta Crystallogr., Sect. B: Struct. Crystallogr. Cryst. Chem. **25**, 925 (1969).
[23] W. Kohn and L. J. Sham, Phys. Rev. **140**, A1133 (1965).
[24] P. E. Blöchl, Phys. Rev. B **50**, 17953 (1994).
[25] G. Kresse and J. Furthmüller, Comp. Mat. Sci. **6**, 15 (1996).
[26] G. Kresse and D. Joubert, Phys. Rev. B **59**, 1758 (1999).
[27] J. P. Perdew, K. Burke, and M. Ernzerhof, Phys. Rev. Lett. **77**, 3865 (1996).
[28] E. T. McClure, M. R. Ball, W. Windl, and P. M. Woodward, Chem. Mater. **28**, 1348 (2016).
[29] C. N. Savory, A. Walsh, and D. O. Scanlon, ACS Energy Lett. **1**, 949 (2016).
[30] A. Janotti, J. B. Varley, P. Rinke, N. Umezawa, G. Kresse, and C. Van de Walle, Phys. Rev. B **81**, 085212 (2010).
[31] A. Stroppa and G. Kresse, Phys. Rev. B **79**, 201201 (2009).
[32] W.-J. Yin, T. Shi, and Y. Yan, J. Phys. Chem. C **119**, 5253 (2015).
[33] A. V. Krukau, O. A. Vydrov, A. F. Izmaylov, and G. E. Scuseria, J. Chem. Phys. **125**, 224106 (2006).
[34] E. Greul, M. L. Petrus, A. Binek, P. Docampo, and T. Bein, J. Mater. Chem. A **5**, 19972 (2017).
[35] M. Gajdoš, K. Hummer, G. Kresse, J. Furthmüller, and F. Bechstedt, Phys. Rev. B **73**, 045112 (2006).
[36] M. A. Green, *Third Generation Photovoltaics: Advanced Solar Energy Conversion* (Springer Science & Business Media, Berlin, 2006), Vol. 12.
[37] T. Tiedje, E. Yablonovitch, G. D. Cody, and B. G. Brooks, IEEE Trans. Electron Devices **31**, 711 (1984).